

HALO FORMATION IN INTENSE LINACS

Chiping Chen

Plasma Science and Fusion Center
Massachusetts Institute of Technology
Cambridge, Massachusetts 02139, USA

Abstract

Halo formation is an important issue in the development of high-power accelerators. In this paper, we discuss from the point of view of beam transport the mechanisms of halo formation in root-mean-square (rms) matched, high-brightness, space-charge-dominated beams in periodic focusing transport systems. In particular, it is shown theoretically that an important mechanism of halo formation in rms matched beams is due to chaotic particle motion induced by charge-density fluctuations about the ideal uniform density profile transverse to the direction of beam propagation. Experimental evidence is presented in support of the theoretical predication of halo formation in rms matched beams. Finally, to gain a better understanding of the equilibrium and stability properties of periodic focused intense charged particles, a rigid-rotor Vlasov equilibrium is discussed, and the effect of beam rotation on the phase space structure is studied.

1 INTRODUCTION

The problem of halo formation in intense charged-particle beams has been the subject of recent vigorous theoretical, computational and experimental investigations [1]-[19]. It is of fundamental importance in the development of next generation high-power accelerators for basic scientific research in high-energy and nuclear physics as well as for a wide variety of applications ranging from heavy ion fusion, accelerator production of tritium, accelerator transmutation of nuclear waste, spallation neutron sources, high-power microwave sources, to high-power free-electron lasers. In such high-power accelerators, beam halos must be controlled in order to keep beam losses at minimum.

It is well-known that a space-charge-dominated beam can develop a sizable halo if there is a root-mean-square (rms) mismatch between the beam and the focusing field [2]-[4],[6],[9]-[11]. The mechanism for halo formation in rms mismatched beams has been well described in the particle-core model [3, 6]. When there is a sizable mismatch, the halo can contain a substantial fraction (up to 15%) of the entire beam.

Recently, it has been shown theoretically [5, 8, 14, 15] that in periodic focusing transport systems, charge density fluctuations in rms-matched space-charged-dominated beams can also cause halo formation. An important mechanism of halo formation in rms matched beams has been

identified with chaotic particle motion and nonlinear resonances occurring in the vicinity of the boundary of phase space occupied by the particles in the beam core. Invariant (Kolmogorov-Arnold-Moser) surfaces [20] play an important role in confining halo particles transverse to the direction of beam propagation. Because halos in rms matched beams are relatively tenuous compared with those in rms mismatched beams, experimental observations of halos in rms matched beams require detectors with a wide dynamic range. A recent observation of a halo in an rms matched potassium K^+ ion beam at the 2-MV Heavy Ion Beam Injector Experiment at Lawrence Berkeley National Laboratory (LBNL) [13] provides the first experimental evidence in support of the theoretical prediction [5, 8, 14, 15] of halo formation in rms-matched beams in periodic focusing transport systems.

For beam propagation through a *periodic* focusing transport system with the periodicity length S and the vacuum phase advance σ_0 , a *space-charge-dominated* beam satisfies the condition [15]

$$\frac{SK}{4\sigma_0\varepsilon} > 1, \quad (1)$$

whereas an *emittance-dominated* beam satisfies the condition

$$\frac{SK}{4\sigma_0\varepsilon} \ll 1. \quad (2)$$

In Eqs. (1) and (2), $K = 2q^2 N_b / \gamma_b^3 \beta_b^2 mc^2$ is the normalized beam perveance, ε is the unnormalized rms emittance of the beam, q and m are the particle charge and rest mass, respectively, N_b is the number of particles per unit length, $\beta_b c$ and γ_b are the characteristic velocity and relativistic mass factor of the particles, respectively, and c is the speed of light *in vacuo*. For an electron beam,

$$\frac{SK}{4\sigma_0\varepsilon} = 2.9 \times 10^{-5} \frac{1}{\sigma_0} \left(\frac{S}{\varepsilon_n} \right) \frac{I_b}{\gamma_b^2 \beta_b^2}, \quad (3)$$

where I_b is the electron beam current in amperes, $\varepsilon_n = \gamma_b \beta_b \varepsilon$ is the normalized rms emittance in meter-radians, and S is in meters. For an ion beam,

$$\frac{SK}{4\sigma_0\varepsilon} = 1.6 \times 10^{-8} \frac{1}{\sigma_0 A} \left(\frac{q}{e} \right) \left(\frac{S}{\varepsilon_n} \right) \frac{I_b}{\gamma_b^2 \beta_b^2}, \quad (4)$$

where A and q/e are the atomic mass and magnitude of the charge state of the ion, respectively, I_b is the ion beam

current in amperes, $\varepsilon_n = \gamma_b \beta_b \varepsilon$ is the normalized rms emittance in meter-radians, and S is in meters.

In this paper, we review recent theoretical, computational and experimental investigations of halo formation in high-brightness, space-charge-dominated beams that are rms matched but not fully matched (in terms of phase-space distributions) in periodic focusing transport systems. In particular, it is shown theoretically that the mechanism of halo formation in rms matched beams is due to chaotic particle motion induced by charge-density fluctuations about the ideal uniform density profile transverse to the direction of beam propagation. Experimental evidence is presented in support of the theoretical predication of halo formation in rms matched beams. Finally, to gain a better understanding of the equilibrium and stability properties of periodic focused intense charged particles, a rigid-rotor Vlasov equilibrium is discussed, and the effect of beam rotation on the phase space structure is studied.

2 MECHANISM OF HALO FORMATION IN RMS MATCHED BEAMS

It has been shown theoretically [5, 8, 14, 15] that in periodic focusing transport systems, charge density fluctuations in rms-matched space-charged-dominated beams can also cause halo formation. The mechanism of halo formation in rms matched beams has been identified with chaotic particle motion [20] and nonlinear resonances occurring in the vicinity of the boundary of phase space occupied by the particles in the beam core.

To illustrate the mechanism of halo formation in rms matched beams, we consider test-particle motion in the field configuration consisting of the self-electric and self-magnetic fields of a thin, continuous, intense charge-particle beam and the periodic solenoidal focusing field

$$\mathbf{B}_0(\mathbf{x}) = B_z(s)\mathbf{e}_z - \frac{1}{2}B'_z(s)(x\mathbf{e}_x + y\mathbf{e}_y). \quad (5)$$

Here, \mathbf{e}_x and \mathbf{e}_y are unit Cartesian vectors perpendicular to the beam propagation direction, $s = z$ is the axial coordinate, $x\mathbf{e}_x + y\mathbf{e}_y$ is the transverse displacement from the beam axis at $(x, y) = (0, 0)$, the superscript 'prime' denotes d/ds with $B'_z(s) = dB_z(s)/ds$, and the axial component of magnetic field satisfies

$$B_z(s + S) = B_z(s), \quad (6)$$

where S is the axial period of the focusing field.

The self-electric and self-magnetic fields [21] are readily determined from the steady-state Maxwell equations, assuming the following transverse density profile (Fig. 1)

$$n_b(r, s) = \begin{cases} \hat{n}_b + \delta\hat{n}_b[1 - 2r^2/r_b^2], & r < r_b(s), \\ 0, & r > r_b(s), \end{cases} \quad (7)$$

where $r_b(s) = r_b(s + S)$ is the outermost radius for the rms-matched beam core, $\hat{n}_b(s) = N_b/\pi r_b^2(s)$ (with N_b

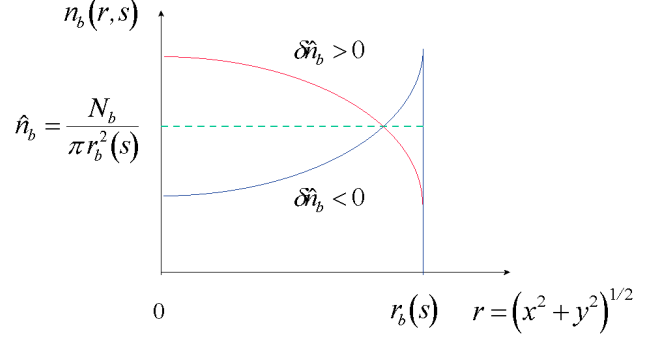


Figure 1: Transverse density profile described by Eq. (7).

being the number of particles per unit axial length), and $\delta\hat{n}_b(s) = \delta N_b/\pi r_b^2(s)$ is a measure of beam density fluctuations. The outermost beam radius $r_b(s)$ can be determined from the rms envelope equation. Note that the Kapchinskij-Vladimirskij (KV) beam equilibrium [22] corresponds to $\delta\hat{n}_b = 0$.

It can be shown that in the Larmor frame of reference [23], the transverse equations of motion for a test particle in the combined periodic solenoidal and self fields are expressed as [15]

$$\frac{d^2x}{ds^2} + \kappa_z(s)x + \frac{q}{\gamma_b^3 \beta_b^2 mc^2} \frac{\partial}{\partial x} \phi^s(x, y, s) = 0, \quad (8)$$

$$\frac{d^2y}{ds^2} + \kappa_z(s)y + \frac{q}{\gamma_b^3 \beta_b^2 mc^2} \frac{\partial}{\partial y} \phi^s(x, y, s) = 0, \quad (9)$$

where $\kappa_z(s) = [qB_z(s)/2\gamma_b \beta_b mc^2]^2$, and the self-field potential ϕ^s is defined by

$$\phi^s = \begin{cases} -q(N_b + \delta N_b)r^2/r_b^2 + q\delta N_b r^4/2r_b^4, & r < r_b(s), \\ -q(N_b + \delta N_b/2) - 2qN_b \ln[r/r_b], & r > r_b(s). \end{cases} \quad (10)$$

Figure 2 shows a Poincare surface-of-section plot in the phase space (x, x') for 2000 test-particle trajectories moving through 20 periods of a step-function lattice with filling factor η for a beam with a hollow density profile. The test particles are loaded initially on a circle defined by

$$W(x, y = 0, x', y' = 0, s = 0) = 1, \quad (11)$$

where W is defined in [15]. The Poincare surface-of-section plot is generated by plotting the positions and momenta of the test particles as they pass through the lattice points $s/S = 0, 1, 2, \dots, 20$. In Fig. 2, x and x' are scaled by the multiplication factors $r_b^{-1}(0)$ and $r_b(0)x'/4\varepsilon_m$, respectively, where $\varepsilon_m = (1 + 2\delta\hat{n}_b/3\hat{n}_b - \delta\hat{n}_b^2/3\hat{n}_b^2)^{-1}\varepsilon$. There is a pair of stable and unstable fixed points at the edge of the beam, i.e., at $x/r_b = \pm 1$ in the phase space. The unstable fixed point is located inside the beam,

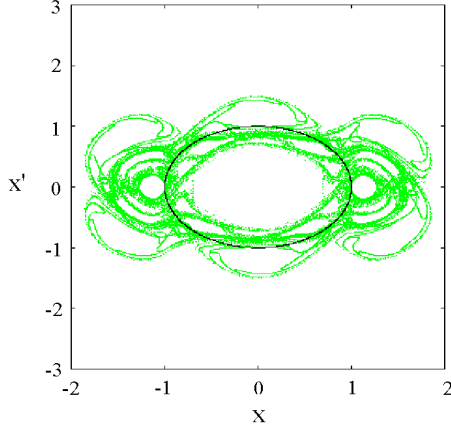


Figure 2: Poincare surface-of-section plot in the phase space (x, x') for 2000 test particles moving through 20 lattice periods. Here, the choice of system parameters corresponds to $\eta = 0.2$, $\sigma_0 = 88.8^\circ$, $SK/4\sigma_0\varepsilon = 6.45$, and $\delta\hat{n}_b/\hat{n}_b = -0.95$.

whereas the stable fixed point and associated island are located outside of the beam. Because of the symmetry in the underlying equations of motion (8) and (9), there is another pair of stable and unstable fixed points at $(x, x') \cong (-1, 0)$. These fixed points, which correspond to periodic solutions of the equations of motion (8) and (9), are induced by excessive space-charge at the edge of the hollow beam. Associated with the two unstable fixed points is a thin chaotic layer (separatrix) which occupies both the region with $W < 1$ and the region with $W > 1$ in the phase space. Particles in this thin chaotic layer can cross the beam envelope, forming a halo around a dense core of beam determined by $W \leq 1$ in the phase space. Although the chaotic layer has a sizable excursion along the x' -axis, it extends to $x/r_b \cong 1.8$ along the x -axis. Therefore, the halo size in this case is about 1.8 times the beam core radius. Because the chaotic layer is thin, the particle density in the halo region is expected to be very tenuous compared with that in the core region.

Shown in Fig. 3 as the dashed and bolded solid curves are, respectively, examples of regular and chaotic trajectories for the same choice of system parameters shown in Fig. 2. In Fig. 3, s is scaled by the multiplication factor S^{-1} , and both x and r_b are scaled by the multiplication factor $(4g\varepsilon S)^{-1}$, where $g = (1 - \delta\hat{n}_b/\hat{n}_b)^{-1}$. The regular trajectory is initialized well inside the beam envelope with $x' = 0$, whereas the chaotic trajectory is initialized near the unstable fixed point with $x' = 0$. Also shown in Fig. 3 as the two solid curves are the outermost periodic boundaries $\pm r_b(s)$ of the rms-matched beam core. The chaotic trajectory intersects the beam core envelope approximately at the thirteenth period of the focusing channel.

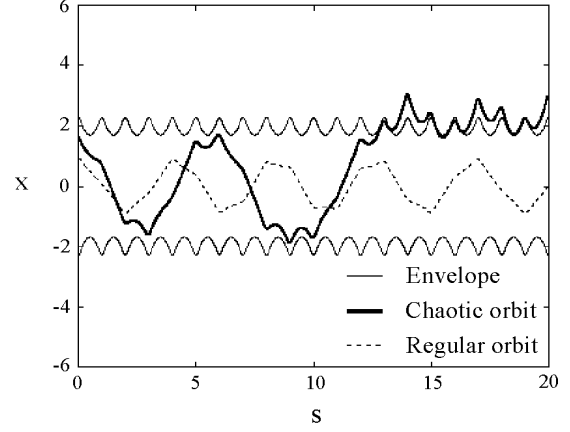


Figure 3: Shown as the dashed and bolded solid curves are, respectively, regular and chaotic trajectories for the same choice of system parameters shown in Fig. 2. Also shown as the two solid curves are the outermost periodic boundaries of the rms-matched beam core. The chaotic trajectory intersects the beam core envelope approximately at the thirteenth period of the focusing channel.

3 COMPARISON BETWEEN THEORY AND EXPERIMENT

Experimental evidence of halo formation has been observed in a space-charge-dominated potassium (K^+) ion beam in the 2-MV Heavy Ion Beam Injector Experiment at the Lawrence Berkeley National Laboratory (LBNL) [13]. In this experiment, a potassium ion beam was extracted from a 1-MV diode. The beam was then accelerated and transversely focused by four electrostatic quadrupoles (which correspond to two periods in a periodic focusing transport system). The four electrostatic quadrupoles add a total of 1 MeV to the ions at the end of the injector. Table 1 gives the basic system parameters measured at the end of the injector. The measured density profile at the end of the injector shows a density depression on the beam axis, and a halo extending 1.47 times the core envelope. The halo was tenuous, containing about 2% of the ions in the beam. A detailed description of the experimental setup and measurements can be found in [13].

A comparison between theory and experiment has been made. In the theoretical analysis, the electrostatic quadrupoles are treated as an alternating-gradient focusing system but the effect of acceleration is ignored. The elliptical cross section of the beam is incorporated. The transverse beam density profile is assumed to be

$$n_b(x, y, s) = \begin{cases} \hat{n}_b + \delta\hat{n}_b(1 - 2T), & T < 1, \\ 0, & T > 1, \end{cases} \quad (12)$$

where $T(x, y, s) = x^2/a^2(s) + y^2/b^2(s)$, and $a(s) = b(s + S)$ and $b(s) = b(s + S)$ are the outermost core envelopes in the x - and y -directions, respectively. For an rms matched

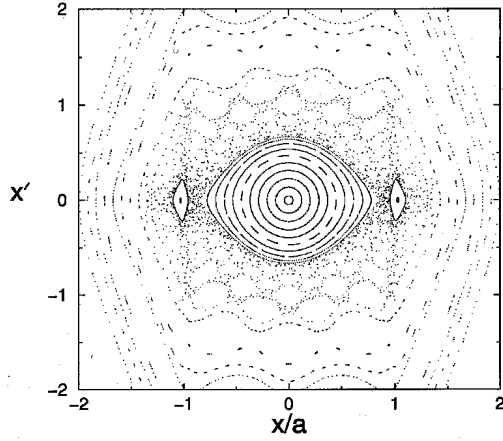


Figure 4: Poincaré surface-of-section plot in (x, x') phase space for 41 test particles in a nonuniform density beam. Here, the choice of system parameters corresponds to $\sigma_0 = 70^\circ$, $\eta = 0.5$, $SK/4\varepsilon_x = 16$, $\varepsilon_x = \varepsilon_y$, and $\delta\hat{n}_b/\hat{n}_b = -0.2$.

beam, $a(s)$ and $b(s)$ are determined from the rms envelope equations.

Figure 4 shows the overall phase space structure for test-particle motion in a Poincaré surface-of-section plot for the nonuniform density beam. The choice of system parameters used to generate Fig. 4 is listed in Table 2, corresponding to the basic system parameters listed in Table 1. Shown in Fig. 4 are the trajectories

Table 1. Basic Parameters of the LBNL Experiment

Ion Type	Potassium
Beam Current	0.79 A
Ion Kinetic Energy	2.0 MeV
$4 \times$ Normalized Emittance	0.6 mm-mrad
Electrostatic Quad Period	0.8 m
Vacuum Phase Advance	70°

Table 2. Parameters in the Simulation

Vacuum Phase Advance σ_0	70°
Lattice Filling Factor η	0.5
$SK/4\sigma_0\varepsilon_x$ ($\varepsilon_x = \varepsilon_y$)	13.1
$\delta\hat{n}_b/\hat{n}_b$	-0.2

of 41 particles as they pass through the lattice points at $s = 0, S, 2S, \dots, 400S$. The initial conditions for these particles are: $x(0)/a(0) = 0.1n$, $y(0) = 0$, and $x'(0) = y'(0) = 0$, where $n = 0, \pm 1, \dots, \pm 20$. Note that for $y(0) = 0 = y'(0)$, the motion in (x, x') phase space is decoupled completely from that in (y, y') phase space. In Fig. 4, the vertical axis is scaled by the dimensionless quantity $(S/4g\varepsilon_x)^{1/2}$. There are two stable period-one orbits near the edge of the beam at $(x, x') \cong (\pm a, 0)$. These stable period-one orbits are accompanied by two *unstable* period-one orbits located approximately at $(x, x') \cong$

$(\pm 0.9a, 0)$. It is the chaotic separatrix associated with the unstable period-one orbits that is responsible for particle escape from the beam interior to form a halo.

For beam propagation through several lattice periods, the Kolmogorov-Arnold-Moser (KAM) surface [20] at $(x, 0) = (\pm 1.42a, 0)$ is expected to determine the halo size. Therefore, the halo size in the x -direction is estimated to be $x_{\text{halo}} = 1.42a$, which is in good agreement with the measured halo size $x_{\text{halo}} = 1.47a$ [13]. Detailed numerical studies of the beam dynamics with a properly chosen initial distribution function show that a relatively small fraction (4%) of the particles in the beam become halo particles after five lattice periods, and the experimental measurements indicate that about 2% of the particles become halo particles in one lattice period.

4 RIGID-ROTOR VLASOV EQUILIBRIUM

The results presented in Secs. 2 and 3 show that charge-density fluctuations about the ideal uniform density profile induce chaotic particle motion and halo formation in rms matched space-charge-dominated beams in periodic focusing transport systems. Therefore, it is important to gain a better understanding of the equilibrium and stability properties of periodically focused beams. In this regard, we discuss a rigid-rotor Vlasov equilibrium [24, 25] discovered recently for intense beam propagation through a periodic solenoidal magnetic field.

The rigid-rotor Vlasov equilibrium distribution function can be expressed as [24, 25]

$$f_b^0(R, P_R, P_\Theta) = \frac{N_b}{\pi^2 \varepsilon_T} \delta \left[P_R^2 + \frac{P_\Theta^2}{R^2} + R^2 + 2\omega_b P_\Theta - (1 - \omega_b^2) \varepsilon_T \right]. \quad (13)$$

In Eq. (13), $\omega_b = \text{const.}$ ($-1 < \omega_b < 1$) is a parameter measuring beam rotation relative to the Larmor frame. The normalized canonical phase-space variables $(R, \Theta, P_R, P_\Theta)$ are related to the Larmor-frame phase-space variables $(r, \theta, P_r, P_\theta)$ by

$$R = \frac{\sqrt{\varepsilon_T}}{r_b(s)} r, \quad \Theta = \theta, \quad (14)$$

$$P_R = \frac{1}{\sqrt{\varepsilon_T}} \left[r_b(s) \frac{d}{ds} r - r \frac{d}{ds} r_b(s) \right], \quad P_\Theta = P_\theta. \quad (15)$$

It can be shown that $n_b(r, s) = \int dx' dy' f_b^0$ is indeed identical to the step-function density profile defined in Eq. (7) with $\delta\hat{n}_b = 0$. It can also be shown that the well-known KV equilibrium corresponds to the special case with $\omega_b = 0$. Finally, a recent analysis [26] shows that beam rotation with $\omega_b \neq 0$ reduces the degree of chaotic behavior in phase space.

5 CONCLUSIONS

We have discussed several important mechanisms of halo formation in high-brightness, space-charge-dominated beams from the point of view of beam transport. In particular, it has been shown theoretically that the mechanism of halo formation in root-mean-square (rms) matched beams is due to chaotic particle motion induced by charge-density fluctuations about the ideal uniform density profile transverse to the direction of beam propagation. Experimental evidence is presented in support of the theoretical prediction of halo formation in rms matched beams. Finally, to gain a better understanding of the equilibrium and stability properties of periodic focused intense charged particles, a rigid-rotor Vlasov equilibrium is discussed, and the effect of beam rotation on the phase space structure is studied.

6 ACKNOWLEDGMENTS

The author wishes to thank R. C. Davidson, Y. Fink, R. A. Jameson, R. Pakter, Q. Qian, and S. S. Yu for their contributions. This work was supported by the Department of Energy, High-Energy Physics Division under Grant No. DE-FG02-95ER40919, Air Force Office of Scientific Research under Grant No. F49620-97-1-0325, and Princeton Plasma Physics Laboratory under Subcontract No. S-03834-K.

7 REFERENCES

- [1] *Space Charge Dominated Beams and Applications of High Brightness Beams*, edited by S. Y. Lee, AIP Conf. Proc. **377** (AIP, New York, 1996).
- [2] I. Haber, D. Kehne, M. Reiser, and H. Rudd, Phys. Rev. **A44**, 5194 (1991).
- [3] J. S. O'Connell, T. P. Wangler, R. S. Mills, and K. R. Crandall, Proc. 1993 Part. Accel. Conf. (IEEE Service Center, Piscataway, New Jersey, 1993), Vol. 5, p. 3657.
- [4] C. Chen and R. C. Davidson, Phys. Rev. Lett. **72**, 2195 (1994); Phys. Rev. **E49**, 5679 (1994).
- [5] Q. Qian, R. C. Davidson, and C. Chen, Phys. Plasmas **1**, 3104 (1994).
- [6] R. L. Gluckstern, Phys. Rev. Lett. **73**, 1247 (1994).
- [7] L. M. Lagniel, Nucl. Instrum. Methods Phys. Res. **A345**, 1576 (1995).
- [8] Q. Qian, R. C. Davidson, and C. Chen, Phys. Plasmas **2**, 2674 (1995).
- [9] C. Chen and R. A. Jameson, Phys. Rev. **E52**, 3074 (1995).
- [10] S. Y. Lee and A. Riabko, Phys. Rev. **E51**, 1609 (1995).
- [11] I. Haber, *et al.*, in Ref. 1, p. 105.
- [12] F. L. Krawczyk, *et al.*, Proc. 1995 Part. Accel. Conf. (IEEE, Piscataway, New Jersey, 1995), p. 2306.
- [13] S. Yu, S. Eylon, E. Henestroza, and D. Grote, in Ref. 1, p. 134.
- [14] C. Chen, Y. Fink, R. C. Davidson, and Q. Qian, "Halo Formation in RMS Matched Intense Ion Beams," Proc. of the Eleventh Int. Conf. on High Power Particle Beams (Prague, Czech Republic, June 10-14, 1996), p. 1018.
- [15] Y. Fink, C. Chen, and W. P. Marable, Phys. Rev. **E55**, 7557 (1997).
- [16] M. Pabst, K. Bongardt, and A. P. Letchford, in Ref. 1, p. 343.
- [17] R. W. Garnett, *et al.*, in Ref. 1, p. 60.
- [18] R. Pakter and C. Chen, "Emittance Growth and Particle Diffusion Induced by Discrete Particle Effects in Intense Beams," Proc. 1997 Part. Accel. Conf. (1997), p. 1938.
- [19] H. Okamoto and M. Ikegami, Phys. Rev. **E55**, 4694 (1997).
- [20] A. J. Lichtenberg and M. A. Lieberman, *Regular and Chaotic Dynamics*, 2nd ed. (Springer-Verlag, New York, 1992).
- [21] R. C. Davidson, *Physics of Nonneutral Plasmas* (Addison-Wesley, Reading, MA, 1990).
- [22] I. M. Kapchinskij and V. V. Vladimirsij, in *Proceedings of the International Conference on High Energy Accelerators* (CERN, Geneva, 1959), p. 274.
- [23] M. Reiser, *Theory and Design of Charged-Particle Beams* (Wiley & Sons, New York, 1994).
- [24] C. Chen, R. Pakter, and R. C. Davidson, Phys. Rev. Lett. **79**, 225 (1997).
- [25] R. C. Davidson and C. Chen, Part. Accel. **59**, 175 (1998).
- [26] C. Chen, R. Pakter, and R. C. Davidson, "Phase Space Structure for Intense Charged-Particle Beams in Periodic Focusing Transport Systems," submitted for publication (1998).